SLAC-R-1061

Report on Proton and Ion Beam measurements at the Matter in Extreme Condition (MEC) end station at SLAC National Accelerator Laboratory

M. Gauthier, S. Goede, W. Schumaker, C. Roedel, E. Galtier, and S. H. Glenzer

SLAC National Accelerator Laboratory, Stanford University, Stanford, CA 94309

This material is based upon work supported by the U.S. Department of Energy,
Office of Science, Office of Basic Energy Sciences, under Contract No. DE-AC02-76SF00515 and FES.

Report on Proton and Ion Beam measurements at the Matter in Extreme Condition (MEC) end station at SLAC National Accelerator Laboratory

M. Gauthier, S. Goede, W. Schumaker, C. Roedel, E. Galtier, and S. H. Glenzer
[1]SLAC National Accelerator Laboratory, CA 94025 Menlo Park

We report on MeV ion beams produced with high-repetition rates of 1 Hz at the MEC end station at SLAC National Accelerator Laboratory. These data were obtained during the commissioning beam time of the new 30TW laser. After describing the experimental set-up, the laser conditions and the target diagnostics, ion beam spectra measured for different foil thicknesses and laser intensities will be presented and discussed. These results are subsequently compared with results from cryogenic hydrogen jets at MEC in January 2015.

I. Introduction

Ion acceleration from high-intensity laser-plasma interactions has attracted great interest due to the potential applications such as ion beam therapy of cancer [Taj2009] or fast ignition [Rot2001]. They are also currently used for proton radiography, imaging, stopping power measurements, and isochoric heating of fusion plasmas, and warm dense matter studies. In the past two decades several different acceleration mechanisms have been proposed and partially demonstrated [Mac2013]. Proton energies up to 65 MeV have been demonstrated using thin foil targets and target normal sheath acceleration (TNSA) [Mora2003, Hatchett2000; Wilks1992]. However, the progress in laser-driven ion acceleration is much slower than initially anticipated. Most of the requirements for applications in terms of ion energy, conversion efficiency, spectral width, brilliance and suitability for high-repetition rate operations have not been achieved yet. To overcome the limitations of TNSA, recent studies using particle-in-cell (PIC) simulations have shown that using higher laser intensities and tailored high-density targets can access favorable regimes of laser ion acceleration described as Radiation Pressure Acceleration (RPA) [Robinson2008], Breakout Afterburner Acceleration (BOA) [Yin2006] and Collision-less Shock Acceleration (CSA) [Haberberger2012].

The High Energy Density Science Group at SLAC National Accelerator Laboratory is currently developing a new cryogenic hydrogen target. Due to its high purity, and limited size, this unique target is highly appropriate to study those new accelerations regime and the physics that governs them. In addition, its stability and compatibility to high repetition rates (1Hz demonstrated) makes this target very suitable for experiment at the MEC end station at SLAC National Accelerator Laboratory, combining a 30TW, 1Hz high-intensity laser and the 120 Hz x-ray Free Electron Laser (FEL). In the scope of these

unique experimental capabilities, it is of high importance to characterize the MEC laser experiment conditions, especially its intensity, contrast, and efficiency at accelerating ions through a well-assessed acceleration regime such as TNSA as much as testing and calibrating the new high-repetition rate ion diagnostic that was implemented at MEC.

II. Experimental set-up

A. MEC Laser

The Commissioning experiment was carried out using the MEC short pulse laser at SLAC National Accelerator Laboratory working in the CPA mode at a wavelength $\lambda =$ 800 nm. During the commissioning, the laser was operated at 1 Hz, 20 TW. Indeed, only the first two amplifiers were used delivering energies of, respectively, 0.9 - 1.2 J, and 0.56 - 0.9 J measured before and after compression to 50 fs (see fig. 1).

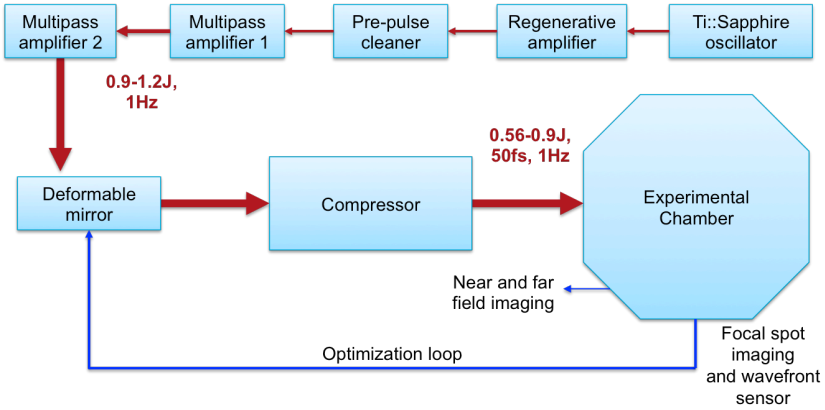

Figure 1: 30 TW MEC laser system and experimental set-up used during the commissioning beam time. The laser beam quality was optimized through an optimization loop between the deformable mirror and the image of the OAP focal spot.

The ASE measured using a fast photodiode before the entrance of the target chamber was estimated below 10^{-9} (see fig. 2a). Due to some technical issues, we were not able to obtain any recent 3rd order autocorrelator trace (fig. 2b shows the trace measured in 2014). It could have provided us some indication about the laser pre-pulse, which is of the greatest importance in ion acceleration physics. Note, that a plasma mirror set-up was implemented to improve the laser contrast but not used during the commissioning beam time due to a lack of facility access time.

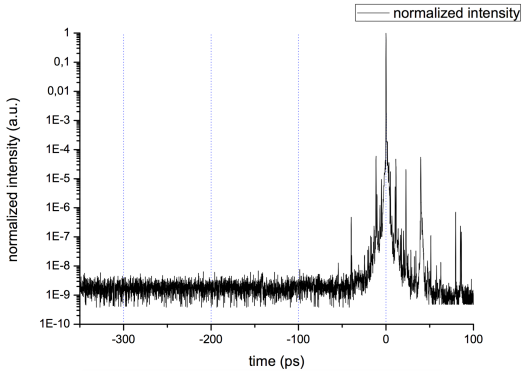

Figure 2: measurements of MEC laser pulse contrast.

The laser beam was focused onto a metallic or plastic thin foil target using a 178 mm focal length, gold coated, 45°off-axis parabola (OAP) to a 6 to 10 µm diameter focal spot full width of maximum (FWHM) after optimization with the deformable mirror. The intensity on target was estimated between 1 and 5.10^{19} W/cm^2 varying with shot-to-shot energy and focal spot quality fluctuations.

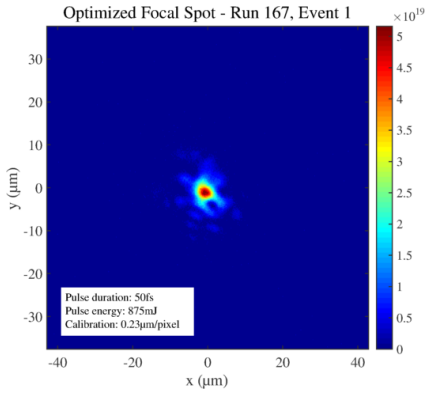

Figure 3: Typical laser focal spot measured at MEC.

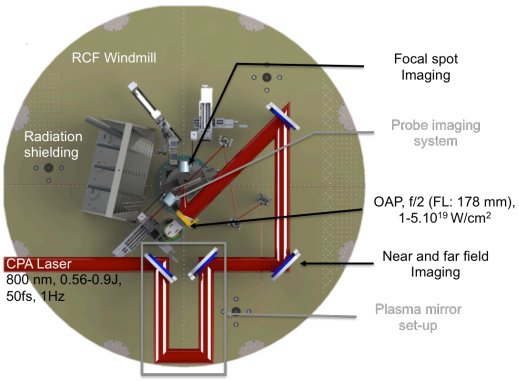

Figure 4: Experimental set-up.

B. Interaction diagnostics

In order to diagnose, the high-intensity laser-plasma interaction, we used two main diagnostics. Scintillators located in the forward direction of the laser were measuring the amount of radiations coming from hot electrons and gammas generated during the interaction. This diagnostic provides a qualitative and relative measurement of the laser intensity on target.

A Thomson Parabola, TP, (see fig. 5) coupled with radiochromic films (RCFs) stacks (see fig. 6) was recording the ion beam spectra in the target surface normal direction making an angle of 22.5° with respect to the laser forward direction (see fig. 7).

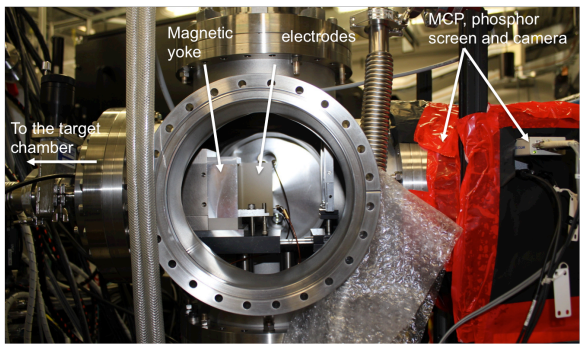

Figure 5: Image of the Thomson Parabola.

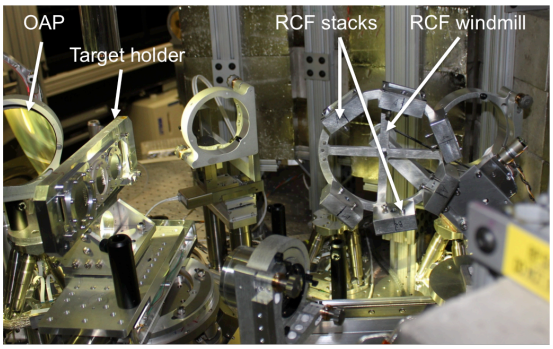

Figure 6: Image of the RCF windmill.

The RCFs stack was located at 3 cm from the interaction point facing the rear side of the target foil, covering more than 45° half-angle cone of proton emission. There were mounted on a motorized windmill in order to replace them in order to avoid having to open the chamber between two shots. Their purpose was to provide an energetically and quantitatively resolved map of the laser-produced proton emission. The RCFs were protected from the laser light and UV radiation by 13µm thick aluminum foil.

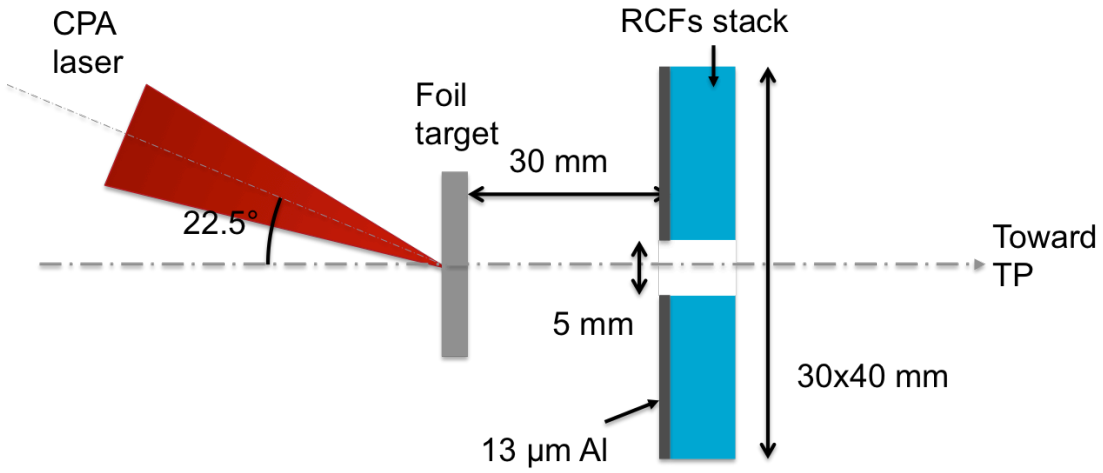

Figure 7: Localization of the RCF stack with respect to the target foil and laser beam axis

The Thomson Parabola (see fig. 8) aims at measuring the energetic spectrum of the different ions contained in the laser-produced ion beam. In practice, only different charge-to-mass ratio ions can be separated. Each ion of the beam is deflected (along the x-axis see fig. 8) by a constant magnetic field built up by two magnets inside a yoke, the deflection depending on the energy and the charge-to-mass ratio of the ion. Then each ion passes between two electric plates and the constant electric field deflects it along the orthogonal direction with respect to the previous direction of deflection (along the y-axis see fig. 8), so that the different traces drawn by the deflected ions hitting the detector can be differentiated. In order to retrieve the different spectra from the image obtained on the detector, we use the theoretical equations of the ion motions.

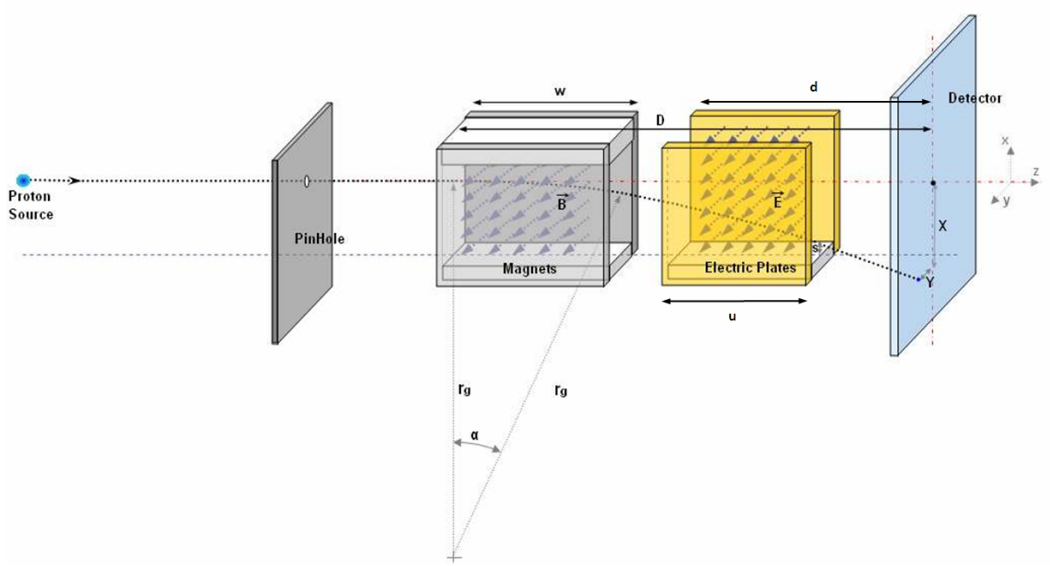

Figure 8: Schematic of the Thomson Parabola.

In our experiment, the ion are passing through a 500-µm diameter pinhole made of 1 mm thick Cu, positioned 98 cm away from the interaction, collecting a solid angle of 8.1 10^{-5} sr. The magnets (w = 50 mm) and electrodes (d = 80 mm) produce, respectively, a 0.4 T magnetic field (according to the producer) and a ~ 4 - 6 kV/cm electric field. The deflected ions deposit their energy on a MCP, Micro Channel Plate (D = 280 mm, d = 151 mm) followed by a phosphor screen, fed respectively by 1650 V and 4000 V, that amplifies the original signal produced by the ions. Our 2 stages MCP can amplify from 10^5 to 10^7 depending on the voltage applied, in our case a few 10^6. Eventually an OPAL2000 Camera records the image printed on the phosphor screen (see fig. 9). The 80-100µm-resolution image on the phosphor screen remains from 2-4 µs, making our diagnostics highly compatible with high repetition rate. Note that the high voltage of the MCP requires a vacuum typically below 10^{-6} mBar to avoid noise and high voltage tripping. In our set-up, a differential pumping system made of 1 mm diameter pinhole was implemented between the TP chamber and the target chamber to ensure a strong mitigation of any low quality vacuum of the target chamber that, for instance, occurs when the cryogenic hydrogen target is used.

In order to evaluate the error bar in the spectrum on the energy, one has to take into account the resolution of all the different parts that compose the Thomson Parabola:

1) Uncertainty in the magnetic field strength and non-uniformity: around +/- 0.01 T after calibration
2) Size of the pinhole: the different ion spectra are convolved with the pinhole size reducing the precision in energy. On the other hand, a larger pinhole increases the

collecting solid angle making the diagnostic more sensitive to ions: here +/- 250 µm

3) Resolution of the imaging camera: here, we computed 76 +/- 1 µm/pixel µm
4) Resolution of the phosphor screen: here, +/- 50 µm (negligible with respect to the resolution of the imaging system)

As shown on fig. 9, for proton energy below 10 MeV, the imprecision in the magnetic field gives a constant relative error bar at 10%. Then, above 10 MeV, the pinhole diameter will limit the resolution; the relative imprecision increases with the energy with for instance a 20% error bar at 50 MeV protons energy.

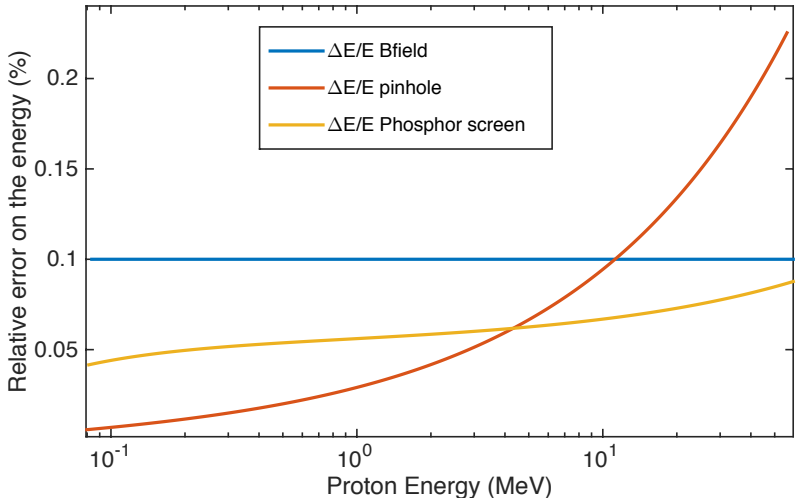

Figure 9: Estimates of the error bar on the energy measured by the Thomson Parabola.

Contrary to single shots ion detectors such as Image plate, Radiochromic films, or CR39 that can be used to obtain absolute ion spectra, published calibration does not exist for MCP-Phosphor screen detectors. Indeed, each set-up has its own advantages, which can vary depending on the imaging system sensibility, MCP gain, or quality of the vacuum in the Thomson Parabola chamber. Furthermore, it is not clear if the amount of signal generated by a proton hit on the MCP varies significantly with the proton energy. One solution is to perform a cross-calibration with one of these (already calibrated) single shot detectors. A CR39 detector (this detector is capable of detecting single proton hit) is located before and close to the MCP (see fig. 10a). A column of holes is drilled along the trace of the protons on the CR39, so that a part of the spectrum is still imprinted in the phosphor screen (see fig10b). Since the proton spectrum evolves smoothly over energy, the signal on each detector can be compared and a calibration counts vs. protons as a function of the proton energy can then be extracted (see for instance fig.11). Note that the MCP efficiency for proton energies in our range of interest is generally assumed linear [H. Schwoerer et al., Nature (London) 439, 445 (2006)].

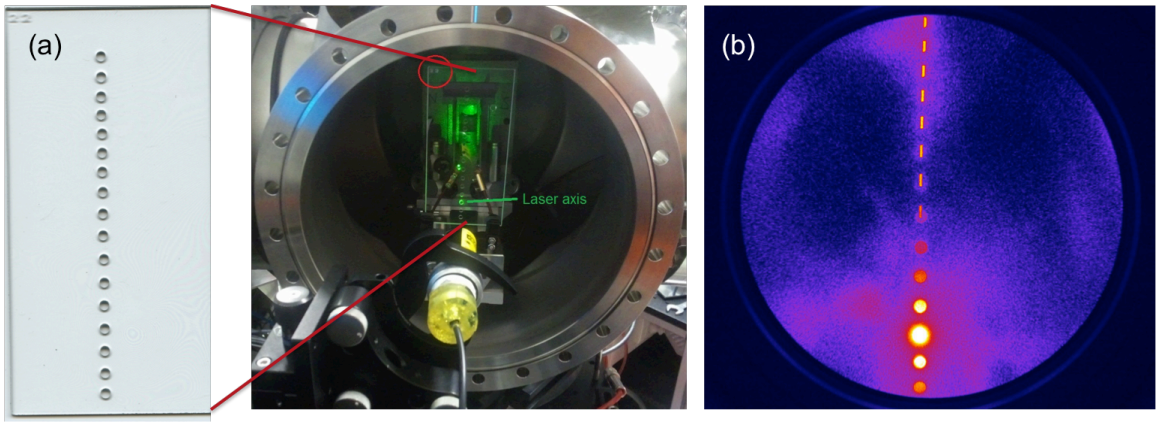

Figure 10: (a) Calibration set-up of the Thomson Parabola used at DRACO (HZDR, Germany); (b) signal recorded on the phosphor screen. Note that this calibration has been performed using a pure proton beam obtained from a cryogenic hydrogen target. As a consequence the electrodes of the Thomson Parabola were turned off making the trace straight on the phosphor screen.

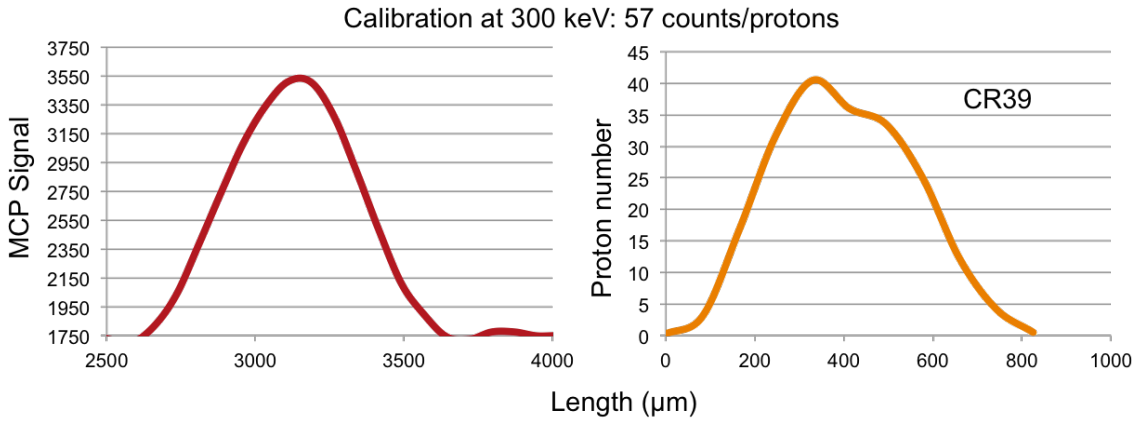

Figure 11: Comparison between the signal on the MCP at ~ 300 keV and the number of proton detected on the CR39 at ~ 300 keV on the same shot; we can deduce that a proton (at 300 keV) hit generates 57 counts on the MCP.

Due to the lack of time and the relative low interest in the actual number of protons produced (we were in the well-known TNSA regime), such calibration has not been performed during the commissioning beam time. Our plan was to rely on the spectrum from the holed RCF stacks (see fig.7) and to compare them with the spectrum of the proton beam passing through the hole. Unfortunately, the maximum proton energy reached during the commissioning beam time was almost always below 1 MeV; the protons were blocked by the aluminum filter in front of the RCF stack.

Eventually, in order to extract more efficiently and quickly the recorded spectra, we have developed a Matlab interface that traces directly on the image the different ion traces depending on the TP parameters (distance and fields) and then extracts their spectra (see fig. 10). In the scope of high repetition rate experiment, we plan on

implementing a function to extract automatically the spectrum using constant TP parameters.

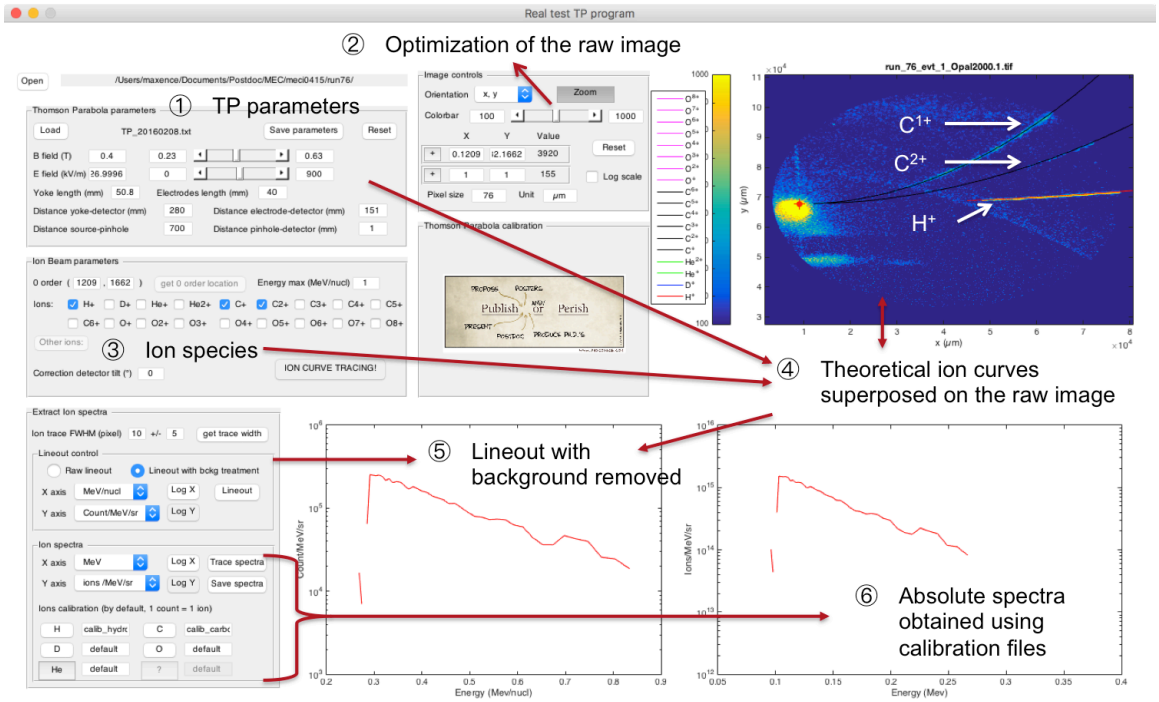

Figure 12: Matlab interface developed to extract ion spectrum.

III. Results

A. Focal scan

Laser-produced ion beams are very sensitive to the laser intensity on target achieved during a shot. Therefore it is of extreme importance to position the target at the maximum laser intensity, i.e. its focal spot, as shown on fig.10. One can observe that the proton energy cut-off is at its maximum when the 12.5 µm aluminum foil is in focus (a). In addition, we note that the highest carbon charge states are obtained at such high intensity (C^{4+}) and that they tend to disappear when the foil is out of focus (b and c). Indeed higher intensity laser pulse produces hot electrons of higher temperature, which in turn generate stronger electrostatic sheath field at the rear target surface capable of ionizing to carbon atoms to higher charge states.

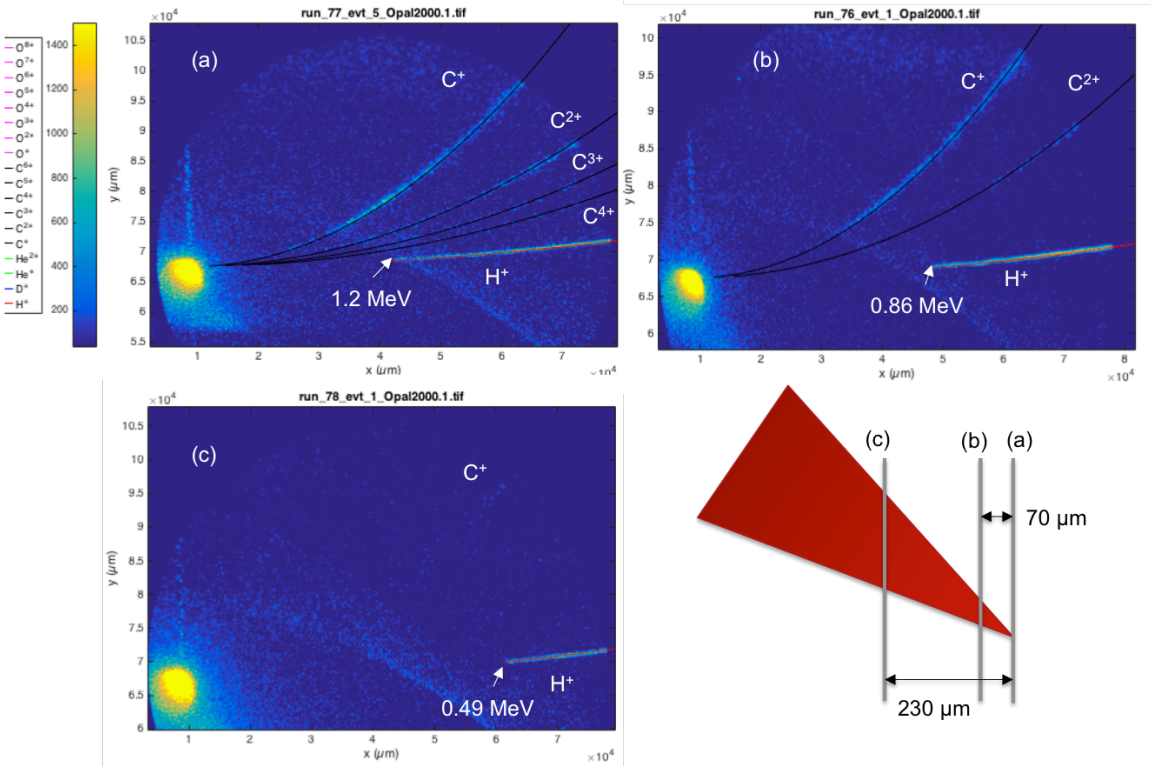

Figure 13: Thomson parabola trace obtained for different position of the target foil with respect to the laser focal spot: (a) in focus, (b) 70 µm defocused, and (c) 230 µm defocused.

On high repetition rate laser system, a common way to find the focus position is to perform a focal scan, i.e., performing shots while spanning the focal region with the foil target and recording the proton energy cut-off. The minimum step size corresponds to the Rayleigh length of the laser, here between 35 to 98 µm depending on the focal spot diameter. The result obtained with a 12.5-µm aluminum foil is shown in fig. 11. Since the maximum carbon ionization charge accelerated during the interaction is characteristic of the electrostatic field strength achieved during the TNSA mechanism, we have separated the shots following the carbon ion highest charge states accelerated.

In parallel to those measurements, we recorded the signal detected by the scintillator in the laser forward direction. As shown in fig. 12, the two curves are in good agreement with each other indicating the same high intensity location, between -1.3 and -1.1 mm. Interestingly, we note that apart from two shots around or above 1 MeV, the peak of energy corresponding to the best focus position is wide from both detectors, i.e. ~ 200-250 µm which is more than twice the Rayleigh length computed from the focal spot image. This observation can be explained by a relatively high pre-pulse expanding the target front surface before the main pulse hits it, but also by a default of planarity of the target foils that will broaden our focal scan.

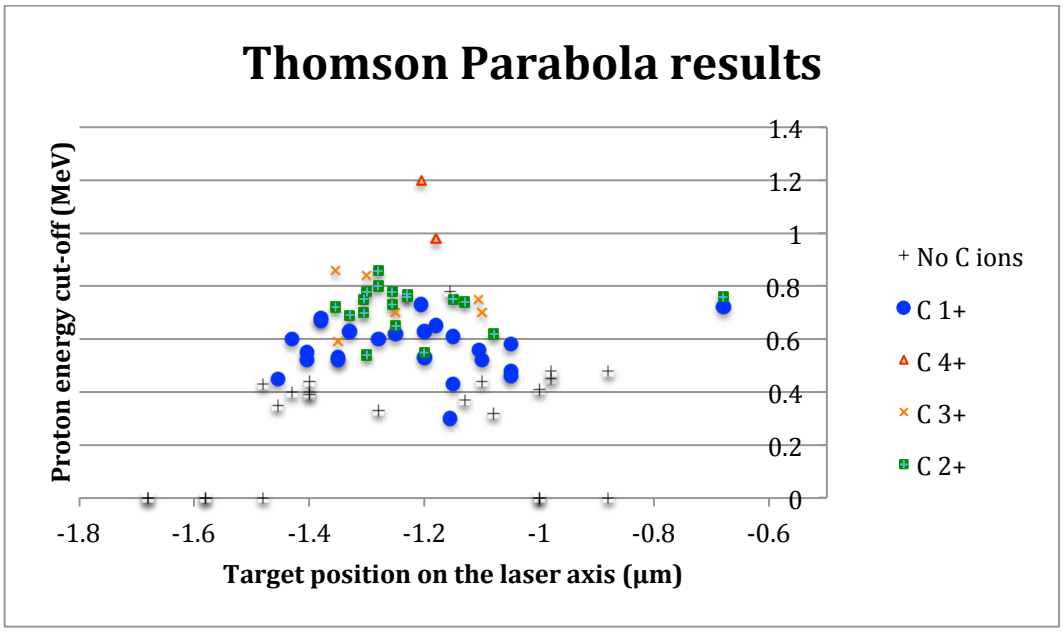

Figure 14: Proton Energy cut-off as a function of the 12.5 µm thick aluminum foil position on the laser axis, recorded during the focal scan.

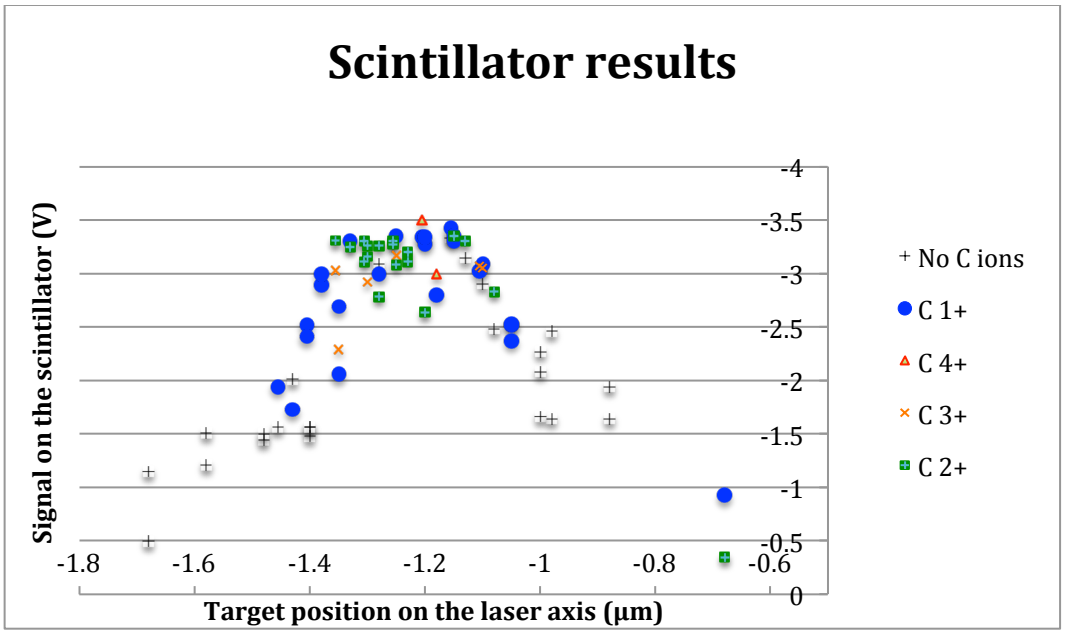

Figure 15: Scintillator signal level as a function of the 12.5 µm thick aluminum foil position on the laser axis, recorded during the focal scan.

B. Thickness scan

Another mean to characterize the laser-interaction is to vary the foil thickness. Indeed high quality laser contrast allows achieving higher proton energy when irradiating thinner targets without expanding their rear surface [M. Kaluza, Phys. Rev. Lett. 93, 045003 (2004)]. Fig. 16 shows the maximum proton energy observed for different target

thickness and material. One can observe that the highest proton energy is obtained for the thickest foils for both aluminum and plastic although energy variations remain marginal between thicknesses. This difference is unlikely due to fluctuations of laser intensity: considering the number of shots performed on each type of foil and that the targets have been irradiated at the same time, we can assume that the target have experienced the same laser conditions.

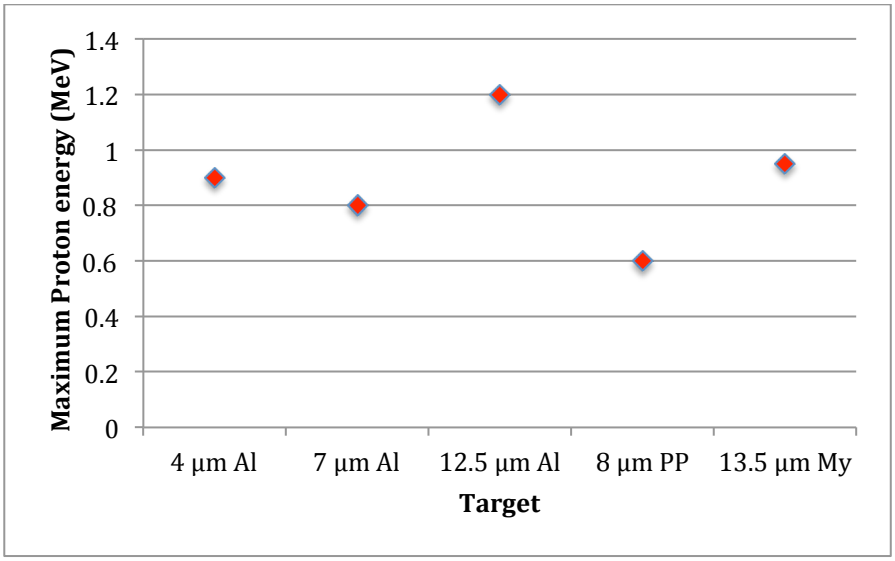

Figure 16: Maximum proton energy (MeV) measured at MEC for different target and thickness.

Furthermore, when comparing those results with the maximum energy cut-off achieved in other facilities (see fig. 17), one finds that the energy achieved at MEC is significantly lower than what has been measured elsewhere with similar laser power. A strong laser pre-pulse could explain these two observations. Indeed, Ceccoti et al., has shown in ref. [T. Ceccoti Phys. Rev. Lett. 99, 185002 (2007)] that under comparable laser conditions (65 fs, 10 TW, $1x10^{19}W/cm^2$) a poor laser contrast ($<10^{-6}$) leads to proton energy cut-off around 1 MeV for target thickness of ~10 µm (optimized target thickness is found to be ~20 µm with 2 MeV protons), while a good contrast ($<10^{-9}$) increases the energy cut-off up to 5 MeV for 0.1 µm thin foils.

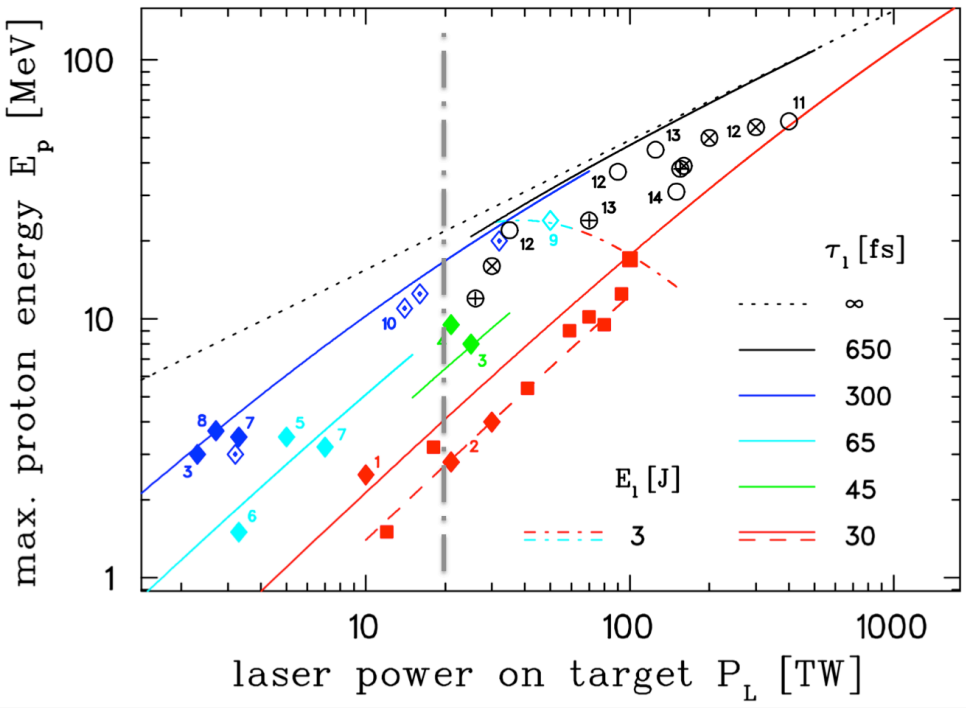

Figure 17: Maximum proton energy scaling law for ultra short pulse (fs) class laser [extracted from K.Zeil et al., New J. Phys. 12, 045015 (2009)].

C. Cryogenic hydrogen experiment at MEC

Let's now compare with the results we achieved using the cryogenic hydrogen jet instead of foils. This experiment took place in January 2015 during an X-ray beam time at MEC. A 50 fs laser pulse was focused onto a cryogenic hydrogen/deuterium jet using a f/3 30° off axis Parabola while a 5.5 keV X-FEL beam was probing it. The main goal of the experiment was to measure the temperature evolution of the electron population through two main diagnostics: a Thomson and a wide-angle x-ray scattering diagnostics. Since the x-ray scattering cross-section from cryogenic hydrogen is very small, a high number of successful shots are necessary to obtain high-quality data with good signal to noise on the x-ray diagnostics.

Further, to separate high-intensity from low-intensity laser-jet hits, a Thomson Parabola located in the laser forward direction was recording the laser-produced ion beam spectrum on each shot. Indeed, a high intensity interaction would induce an energetic proton beam. The three different experimental cases that have been studied during this experiment are the following:

Target	Laser parameter	Repetition rates
Hydrogen	400nm, 50fs, 140-200mJ before compression (~ 100mJ on target)	5 Hz
Deuterium	800nm, 50fs, 140-200mJ before	5 Hz

	compression (~ 100mJ on target)	
Deuterium	800nm, 50fs, 1.4J before compression, (~ 0.7 J on target)	1 Hz

The TP was successfully operated either at 1 or 5 Hz depending on the laser energy. Typical TP traces and spectra recorded for each regime are shown in fig. 18. Contrary to foils where Carbon and Oxygen ions are present, only single species, i.e., protons or deuterons were accelerated.

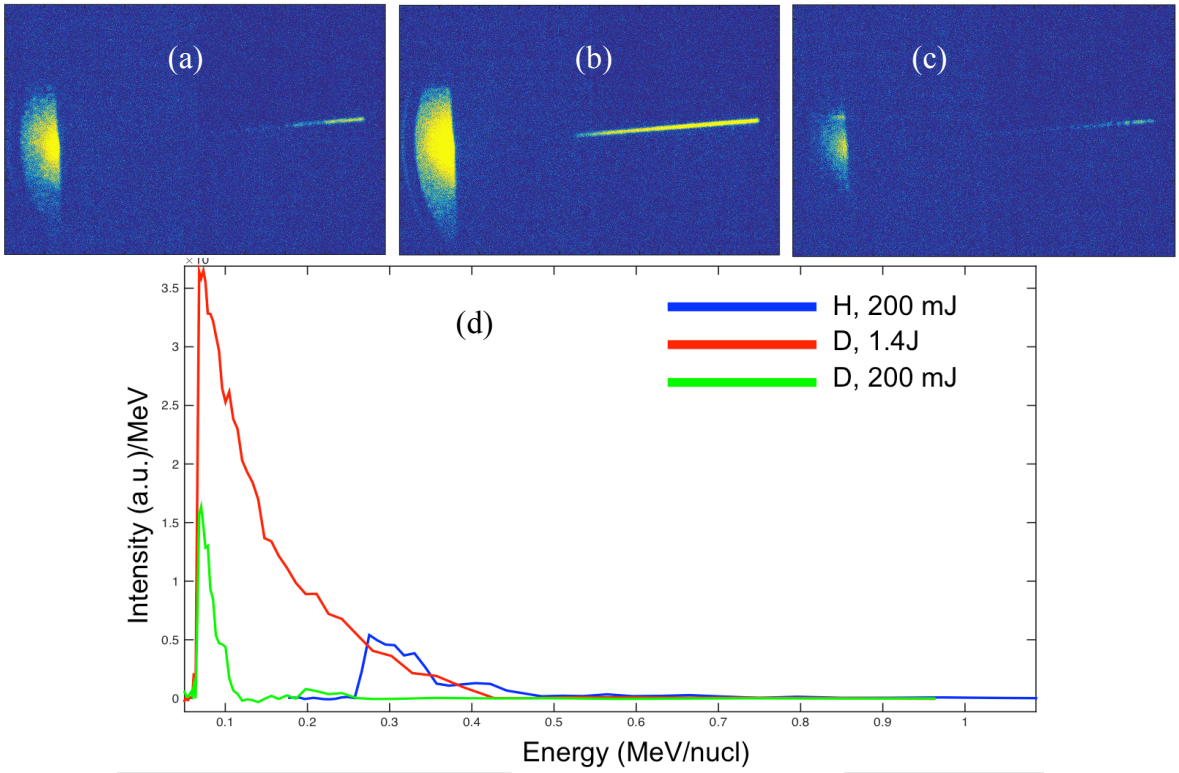

Figure 18: Typical ion trace recorded with (a) hydrogen, 200mJ laser, (b) deuterium, 1.4J laser, (c) deuterium, 200mJ laser, and (d) their respective relative spectra.

The maximum deuteron energy was recorded at ~ 0.25 MeV/nucl and ~ 0.4 MeV/nucl for, respectively, 200 mJ and 1.4 J laser pulse. With their higher charge to mass ratio, protons were accelerated to higher energy values. Although the flux was pretty low (the signal is very close to the MCP noise level) due to the relatively low laser energy, we measured protons up to 0.8 MeV. This result has been crosschecked using a CR39 detector (single ion detection) located in the laser forward direction. A set of filters of different thicknesses was mounted on it in order to roughly determine the maximum proton energy (see fig. 19).

Maximum proton energy between 0.8 and 1.5 MeV (very low flux at high energy)

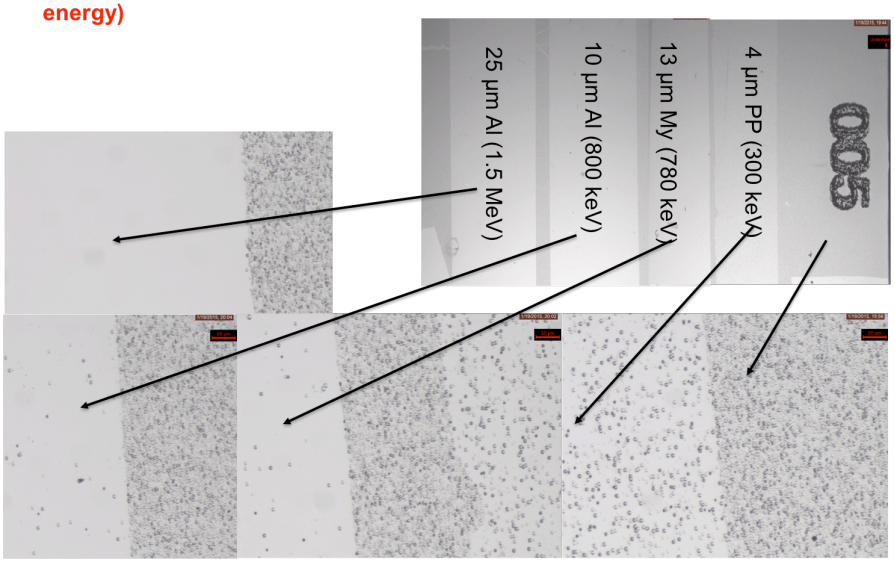

Figure 19: Signal on the CR39 for different energy filters after etching. Proton hits are shown until the 10µm thick aluminum filter that cuts 800 keV. This signal has been integrated over 120 shots.

Using the 5Hz TP traces, we were able to determine that most of the shots were happening at rather low intensity (no proton observed above 300 keV, the low energy detection limit of the TP) with sometimes for some run a 1% hit statistic. The heat generated during high intensity laser interaction with the jet was degrading the pointing stability of the cryogenic jet. This problem has been mostly solved later on during an experiment at DRACO (HZDR), a more powerful laser, where a 10% hit statistic has been demonstrated at 1Hz (repetition rate of the laser system).

IV. Conclusions

During the October 2015 commissioning beam time, we characterized the typical ion beams that can be produced using the 30TW MEC laser beam. We observed that the maximum proton energy cut-off were lower than what has already been achieved with comparable laser systems. The clues collected through a focal and a thickness scan points toward a low pre-pulse contrast. The use of a double plasma mirror could be a solution to reach much higher proton energy.

We have also demonstrated that our new ion diagnostics combined with the MEC laser system is compatible with a 5Hz repetition rate. We were able to diagnose the interaction between the MEC laser and the cryogenic hydrogen jet, determine a high intensity hit statistics, and expose a problem that was occurring after high-intensity shots on the jet.

V. References

1. R. A. Snavely, M. H. Key, S. P. Hatchett, T. E. Cowan, M. Roth, T. W. Phillips, M. A. Stoyer, E. A. Henry, T. C. Sangster, M. S. Singh, S. C. Wilks, A. MacKinnon, A. Offenberger, D. M. Pennington, K. Yasuike, A. B. Langdon, B. F. Lasinski, J. Johnson, M. D. Perry, and E. M. Campbell, Intense high-energy proton beams from petawatt-laser irradiation of solids. Physical Review Letters, 2000. 85(14): p. 2945-2948.

2. A. J. Mackinnon, M. Borghesi, S. Hatchett, M. H. Key, P. K. Patel, H. Campbell, A. Schiavi, R. Snavely, S. C. Wilks, and O. Willi, Effect of plasma scale length on multi-MeV proton production by intense laser pulses. Physical Review Letters, 2001. 86(9): p. 1769.

3. J. Fuchs et al., Laser-driven proton scaling laws and new paths towards energy increase. Nature Physics, 2006. 2(1): p. 48-54.

4. M. M. Borghesi, and M. Passoni, Ion acceleration by superintense laser-plasma interaction. Reviews of Modern Physics, 2013. 85(2): p. 751-793.

5. T. E. Cowan, J. Fuchs, H. Ruhl, A. Kemp, P. Audebert, M. Roth, R. Stephens, I. Barton, A. Blazevic, E. Brambrink, J. Cobble, J. Fernández, J.-C. Gauthier, M. Geissel, M. Hegelich, J. Kaae, S. Karsch, G. P. Le Sage, S. Letzring, M. Manclossi, S. Meyroneinc, A. Newkirk, H. Pépin, and N. Renard-LeGalloudec , Ultralow emittance, multi-MeV proton beams from a laser virtual-cathode plasma accelerator. Physical Review Letters, 2004. 92(20).

6. L. Robson, P.T. Simpson, R.J. Clarke, K.W.D. Ledingham, F. Lindau, O. Lundh, T. McCanny, P. Mora, D. Neely, C.-G. Wahlström, M. Zepf, and P. McKenna, Scaling of proton acceleration driven by petawatt-laser-plasma interactions. Nature Physics, 2007. 3(1): p. 58-62.

7. B. Qiao, M. Zepf, M. Borghesi, B. Dromey, M. Geissler, A. Karmakar, and P. Gibbon, Radiation-Pressure Acceleration of Ion Beams from Nanofoil Targets: The Leaky Light-Sail Regime. Physical Review Letters, 2010. 105(15).

8. L. Yin, B. J. Albright, B. M. Hegelich, and J.C. Fernández, GeV laser ion acceleration from ultrathin targets: The laser break-out afterburner. Laser and Particle Beams, 2006. 24(2): p. 291-298.

9. L. O. Silva, M. Marti, J. R. Davies, R. A. Fonseca, C. Ren, F. S. Tsung, and W. B. Mori, Proton shock acceleration in laser-plasma interactions. Physical Review Letters, 2004. 92(1).

10. F. Fiuza, R. A. Fonseca, J. Tonge, W. B. Mori, and L. O. Silva, Weibel-Instability-Mediated Collisionless Shocks in the Laboratory with Ultraintense Lasers. Physical Review Letters, 2012. 108(23).

11. F. Fiuza, A. Stockem, E. Boella, R. A. Fonseca, L. O. Silva, D. Haberberger, S. Tochitsky, C. Gong, W. B. Mori, and C. Joshi, Laser-Driven Shock Acceleration of Monoenergetic Ion Beams. Physical Review Letters, 2012. 109(21).

12. A. Henig, D. Kiefer, K. Markey, D. C. Gautier, K. A. Flippo, S. Letzring, R. P. Johnson, T. Shimada, L. Yin, B. J. Albright, K. J. Bowers, J. C. Fernandez, S. G. Rykovanov, H.-C. Wu, M. Zepf, D. Jung, V. Kh. Liechtenstein, J. Schreiber, D. Habs, and B. M. Hegelich, Radiation-Pressure Acceleration of Ion Beams Driven by Circularly Polarized Laser Pulses. Physical Review Letters, 2009. 103(24).

13. S. Kar, K. F. Kakolee, B. Qiao, A. Macchi, M. Cerchez, D. Doria, M. Geissler, P. McKenna, D. Neely, J. Osterholz, R. Prasad, K. Quinn, B. Ramakrishna, G. Sarri, O. Willi, X. Y. Yuan, M. Zepf, and M. Borghesi, Ion Acceleration in Multispecies Targets Driven by Intense Laser Radiation Pressure. Physical Review Letters, 2012. 109(18).

14. M. Roth, D. Jung, K. Falk, N. Guler, O. Deppert, M. Devlin, A. Favalli, J. Fernandez, D. Gautier, M. Geissel, R. Haight, C. E. Hamilton, B. M. Hegelich, R. P. Johnson, F. Merrill, G. Schaumann, K. Schoenberg, M. Schollmeier, T. Shimada, T. Taddeucci, J. L. Tybo, F. Wagner, S. A. Wender, C. H. Wilde, and G. A. Wurden, Bright Laser-Driven Neutron Source Based on the Relativistic Transparency of Solids. Physical Review Letters, 2013. 110(4).

15. J. H. Bin, W. J. Ma, H. Y. Wang, M. J. V. Streeter, C. Kreuzer, D. Kiefer, M. Yeung, S. Cousens, P. S. Foster, B. Dromey, X. Q. Yan, R. Ramis, J. Meyer-ter-Vehn, M. Zepf, and J. Schreiber, Ion Acceleration Using Relativistic Pulse Shaping in Near-Critical-Density Plasmas. Physical Review Letters, 2015. 115(6).

16. D. Haberberger, S. Tochitsky, F. Fiuza, C. Gong, R. A. Fonseca, L. O. Silva, W. B. Mori and C. Joshi, Collisionless shocks in laser-produced plasma generate monoenergetic high-energy proton beams. Nature Physics, 2012. 8(1): p. 95-99.

17. M. Borghesi, D. H. Campbell, A. Schiavi, M. G. Haines, O. Willi, A. J. MacKinnon, P. Patel, L. A. Gizzi, M. Galimberti, R. J. Clarke, F. Pegoraro, H. Ruhl, and S. Bulanov, Phys. Plasmas 9, 2214 (2002).

18. S. V. Bulanova, T. Z. Esirkepov, V. S. Khoroshkov, A. V. Kuznetsov, and F. Pegoraro, Phys. Lett. A 299, 240 (2002).

19. M. Roth, T. E. Cowan, M. H.Key, S. P. Hatchett, C. Brown, W. Fountain, J. Johnson, D. M. Pennington, R. A. Snavely, S. C. Wilks, K. Yasuike, H. Ruhl, F. Pegoraro, S. V. Bulanov, E. M. Campbell, M. D. Perry, and H. Powell, Phys. Rev. Lett. 86, 436 (2001).

20. V. Malka, J. Faure, Y. A. Gauduel, E. Lefebvre, A. Rousse, and K. T. Phuoc, Nature Phys. 4, 447 (2008).

21. A. R. Smith, Med. Phys. 36, 556 (2009).

22. V. Malka, S. Fritzler, G. Grillon, J. Chambaret, A. Antonetti, D. Hulin, E. Lefebvre, E. dHumieres, R. Ferrand, C. Albaret, and S. Meyroneinc, Phys. 31, 1587 (2004).

23. S. C. Wilks, A. B. Langdon, T. E. Cowan, M. Roth, M. Singh, S. Hatchett, M. H. Key, D. Pennington, A. MacKinnon, and R. A. Snavely Phys. of Plasmas 8, 542 (2001).

24. T. Esirkepov, M. Borghesi, S. V. Bulanov, G. Mourou, and T. Tajima, Phys. Rev. Lett. 92, 175003 (2004).

25. S. A. Gaillard, T. Kluge, K. A. Flippo, M. Bussmann, B. Gall, T. Lockard, M. Geissel, D. T. Offermann, M. Schollmeier, Y. Sentoku, and T. E. Cowan, Phys. Plasmas 18, 056710 (2011).

26. F. Fiuza, A. Stockem1, E. Boella, R. A. Fonseca, L. O. Silva, D. Haberberger, S. Tochitsky, W. B. Mori and C. Joshi, Phys. Plasmas 20, 056304 (2013).

27. S. S. Bulanov, V. Yu. Bychenkov, V. Chvykov, G. Kalinchenko, D. W. Litzenberg, T. Matsuoka, A. G. R. Thomas, L. Willingale, V. Yanovsky, K. Krushelnick, and A. Maksimchuck, Phys. Plasmas 17, 1 (2010).

28. Tatsufumi Nakamura, Sergei V. Bulanov, Timur Zh. Esirkepov, and Masaki Kando, Phys. Rev. Lett. 105, 135002 (2010).

29. M. H. Helle, D. F. Gordon, D. Kaganovich, Y.-H. Chen, and A. Ting, Proc. SPIE 9514, 951409 (2015).

30. S. Palaniyappan, B. M. Hegelich, H.-C. Wu, D. Jung, D. C. Gautier, L. Yin, B. J. Albright, R. P. Johnson, T. Shimada, S. Letzring, D. T. Offermann, J. Ren, C. Huang, R. Horlein, B. Dromey, J. C. Fernandez, and R. C. Shah, Nature Physics 8, 763 (2012).

31. D. Jung, B. J. Albright, L. Yin, D. C. Gautier, R. Shah, S. Palaniyappan, S. Letzring, B. Dromey, H.-C. Wu, T. Shimada, R. P. Johnson, M. Roth, J. C. Fernandez, D. Habs, and B. M. Hegelich, New J. Phys. 15, 123035 (2013).

32. L. Yin, B. J. Albright, B. M. Hegelich, K. J. Bowers, K. A. Flippo, T. J. T. Kwan, and J. C. Fernandez, Phys. Plasmas, 14, 056706 (2007).

33. B. M. Hegelich, I. Pomerantz, L. Yin, H. C. Wu, D. Jung, B. J. Albright, D. C. Gautier, S. Letzring, S. Palaniyappan, R. Shah, K. Allinger, R. Horlein, J. Schreiber, D. Habs, J. Blakeney, G. Dyer, L. Fuller, E. Gaul, E. Mccary, A. R. Meadows, C. Wang, T. Ditmire, and J. C. Fernandez, New J. Phys. 15, 085015 (2013).

34. Y. Sentoku and A. J. Kemp, J. Comput. Phys., 227, 6846 (2008).

35. R. Mishra, P. Leblanc, Y. Sentoku, M. S. Wei and F. N. Beg, Phys. Plasmas 20, 072704 (2013).

36. P. Mora Phys. Rev. Lett., 90, 185002 (2003).

37. M. Passoni, and M. Lontano, Laser Part. Beams 22, 163 (2004).

38. J. Schreiber, F. Bell, F. Grner, U. Schramm, M. Geissler, M. Schnrer, S. Ter-Avetisyan, B. M. Hegelich, J. Cobble, E. Brambrink, J. Fuchs, P. Audebert, and D. Habs, Phys. Rev. Lett. 97, 045005 (2006).

39. W. L. Kruer and K. Estabrook, Phys. Fluids 0031-9171 28, 430 (1985).

40. J. May, J. Tonge, F. Fiuza, R. A. Fonseca, L. O. Silva, C. Ren, and W. B. Mori, Phys. Rev. E 84, 025401 (2011).

41. A. I. Akhiezer, R. V. Polovin, "Theory of wave motion of an electron plasma" Sov. Phys., JETP 3, 696-705 (1956).

42. P. K. Kaw and J. M. Dawson, Phys. Fluids 13, 472-481 (1970).

43. A.V. Brantov, E. A. Govras, V. Yu. Bychenkov, and W. Rozmus, Phys. Rev. ST Accel. Beams 18, 021301 (2015).

44. E. d'Humires, A. Brantov, V. Yu. Bychenkov, and V. T. Tikhonchuk, Phys. Plasmas 20, 023103 (2013).

45. G. Mourou, T. Tajima, and S. V. Bulanov, Rev. Mod. Phys 78, 309 (2006).

46. H. Daido, M. Nishiuchi, and A. S. Pirozhkov, Rep. Prog. Phys. 75, 056401 (2012).

47. A. Macchi, M. Borghesi, and M. Passoni, Rev. Mod. Phys. 85, 751 (2013).

48. T. Esirkopov, M. Yamagiwa and T. Tajima, Phys. Rev. Lett. 96, 105001 (2006).

49. L. Yin, B. J. Albright, B. M. Hegelich, and J. C. Fernandez, Laser and Particle Beams 24.2 (Jun 2006): 291-298.